The Role of Active Sites Location in Partial Oxidation of Methane to Syngas for MCM-41 Supported Ni Nanoparticles

Chuanmin Ding [1],*, Junwen Wang [1], Yufeng Li [1], Qian Ma [1], Lichao Ma [1], Jing Guo [1], Zili Ma [1], Ping Liu [2] and Kan Zhang [2]

[1] College of Chemistry & Chemical Engineering, Taiyuan University of Technology, Taiyuan 030024, China
[2] Institute of Coal Chemistry, Chinese Academy of Sciences, Taiyuan 030001, China
*   Correspondence: dingchuanmin@tyut.edu.cn; Tel./Fax: +86-0351-6014-498

check for
updates

Abstract: The supporting modes of active metal over mesoporous materials play an important role in catalytic performance. The location of Ni nanoparticles inside or outside the mesoporous channel of MCM-41 has a significant influence on the reactivity in partial oxidation of methane to syngas reaction. The characterization data using different techniques (Transmission Electron Microscope (TEM), X-Ray Diffraction (XRD), N_2 adsorption-desorption, H_2 Temperature-Programmed Reduction (H_2-TPR), and Inductively Coupled Plasma (ICP)) indicated that nickel was located outside the mesoporous channels for the impregnation method (Ni/MCM-41), while nickel was encapsulated within MCM-41 via the one-step hydrothermal crystallization method (Ni-MCM-41). The nickel atoms were mainly dispersed predominantly inside the skeleton of zeolite. When the load amount of Ni increased, both of Ni species inside the skeleton or pore channel of zeolite increased, and the ordered structure of MCM-41 was destroyed gradually. Contributed by the strong interaction with MCM-41, the Ni particles of Ni-MCM-41 were highly dispersed with smaller particle size compared with supported Ni/MCM-41 catalyst. The Ni-MCM-41 displayed higher catalytic performance than Ni/MCM-41, especially 10% Ni-MCM-41 due to high dispersity of Ni. The confinement effect of MCM-41 zeolite also afforded high resistance of sintering and coking for 10% Ni-MCM-41 catalyst. Especially, 10% Ni-MCM-41 catalyst showed outstanding catalytic stability.

Keywords: partial oxidation of methane; sintering and coking resistance; Ni location; confinement effect; MCM-41 zeolite

1. Introduction

While the natural gas industry is relatively underdeveloped, as the predominant component of natural gas, methane is expected to exceed oil by the known enormous reserves. In addition, the recent exploration and production of methane from shale basins have enhanced its competitive advantages. A recent study has estimated that there are 207 trillion cubic meters of recoverable shale gas globally, which impacts the worldwide supply of natural gas [1]. The route of methane to syngas is the most advanced technology to make full use of methane. Wherein, partial oxidation of methane to syngas (POM) stands out due to the merits of the smaller reactor, light heat release and suitable H_2/CO ratio for methanol synthesis [2]. Then, methanol or DME as intermediate is widely applied to produce high value-added chemicals [3–5]. Considering the low cost and relatively high catalytic activity, Ni based catalysts have gained extensive attention. However, Ni based catalysts have suffered from severe sintering and coking, resulting in catalyst deactivation [6,7]. Furthermore, the catalysts might deactivate due to poisoning of the catalyst by impurities of natural gas or bio-methane [8].

In order to improve the stability and performance of the catalyst, variety of strategies have been proposed including introduction of assistant, modification of support, and encapsulation of metal into inert porous material (SiO$_2$, C) [9,10]. These methods have improved the stability of catalyst to some extent, but it could not solve the underlying problems. Therefore, new techniques need to be developed.

The silicate structured mesoporous materials including MCM-41 and SBA-15 with ordered pore structures provide new possibilities to develop promising catalysts with much less transport limitations than microporous zeolites [11]. The metals or metal oxides are incorporated into mesoporous materials to improve their catalytic performances. The synthetic method includes direct synthesis and post-synthesis (impregnation, grafting, etc.) procedures [12–16]. Glucose and β-cyclodextrin modified impregnation methods were employed to realize the high dispersion of Ni on mesoporous MCM-41 for carbon dioxide reforming of methane, which shows higher catalytic activity and stability [17].

It has been reported that the confinement of active metal can prevent sintering and growth-up of carbon fiber. The NiO particles located inside and outside the pore of MCM-41 were used in the pyrolysis catalytic gasification of wood sawdust. The high dispersion of the fine NiO particles inside the pores of the MCM-41 support promoted the catalytic performance [18]. Haller reported that nickel was incorporated by isomorphous substitution of silicon in the MCM-41 silica framework. The prepared catalysts still maintained stable structures even when they were suffering from severe reaction conditions such as CO disproportionation and CO$_2$ methanation [19]. The Ni confined within MCM-41 makes contributions to the improvement of catalytic activity and stability due to highly dispersed and stabilized active centers on the pore wall surface. This anchoring effect promoted the formation of the active Ni nano-clusters with high dispersion and prevented carbon deposition due to the limited growth space of carbon fiber [20,21].

Due to the harsh reaction condition of POM reaction, the sintering of Ni was unavoidable for supported catalyst because of migration of metal atoms at high temperature. Thus, the Ni was incorporated into mesoporous MCM-41 might be a promising candidate with anti-sintering and coking ability. The well-ordered Ni-MCM-41 catalysts with different nickel contents are synthesized by the direct hydrothermal method. According to our knowledge, the reports on the location of Ni and its separate roles within MCM-41 for partial oxidation of methane are few. It is required to be analyzed in this work.

2. Results and Discussion

2.1. Characterization before Tests

2.1.1. Phase Composition

Figure 1 shows the low-angle XRD patterns of fresh Ni/MCM-41 and Ni-MCM-41 catalysts. As shown in Figure 1, a strong diffraction peak occurs at a range of 1°–3° and two weak peaks at 3°–6° for Ni/MCM-41 catalyst, which are attributed to lattice planes of (100), (110), and (200) [22]. The results indicated that the prepared catalysts possessed long-range ordered hexagonal mesoporous skeleton structure of MCM-41. The reason may be that NiO particles dispersed at the surface of catalyst and the framework structure of mesoporous molecular sieve has not been destroyed. For Ni-MCM-41 catalyst, the intensities of all the diffraction peaks were lower compared to Ni/MCM-41. It is speculated that Ni particles are fixed into the MCM-41, resulting in declining crystallinity of molecular sieves [23]. As the amount of Ni increased, the intensity of diffraction peak decreased gradually and shifted toward the low angle with a wider diffraction peak due to the migration of metal ion into the skeleton of molecular sieve [24].
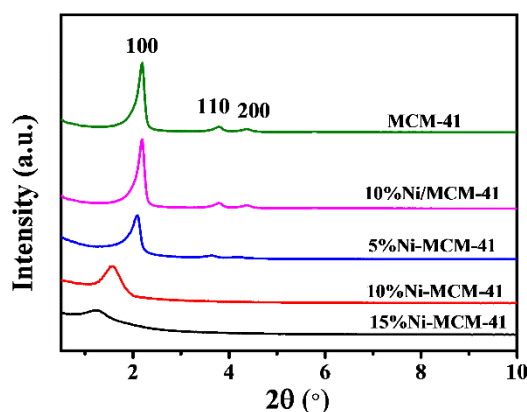
Figure 1. Low-angle XRD patterns of fresh Ni/MCM-41 and Ni-MCM-41 catalysts.

As shown in Figure 2A, there is a significant difference between fresh Ni/MCM-41 catalyst and Ni-MCM-41 catalyst. The obvious diffraction peak of NiO can be observed from 10% Ni/MCM-41 supporting catalyst, further confirming that metal is loaded on the surface of the molecular sieve in the form of NiO [25]. On the contrary, the NiO species is not observed in Ni-MCM-41 catalyst, indicating the high dispersion of metal. The diffraction peak at 34° is assigned to nickel silicate species [26]. Its intensity increases with the increasing of Ni loaded amount. Figure 2B shows the XRD spectrums of Ni/MCM-41and Ni-MCM-41 catalysts after reduction. The diffraction peaks of Ni occurs at all the catalysts. Compared with Ni/MCM-41 catalyst, the intensity of Ni diffraction peaks become lower over Ni-MCM-41 catalysts and increases with the increasing of Ni amount. The result suggests that the Ni nanoparticles can be reduced in spite of zeolite encapsulation. The confinement of channel in MCM-41 contributed to improving dispersion of Ni metal. The average size of Ni particles in reduced 10%Ni-MCM-41 catalyst is around 10 nm by Scherrer equation, which is far smaller than that of 10%Ni/MCM-41 catalyst (23 nm).
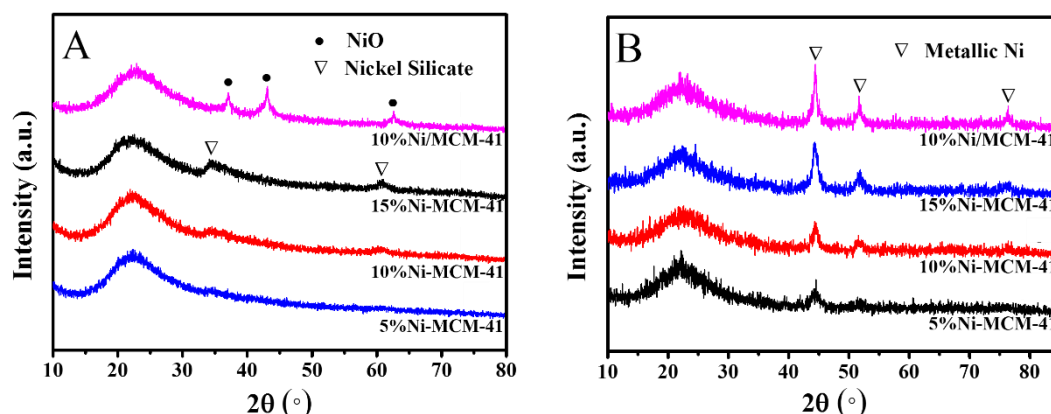

Figure 2. Wide-angle XRD patterns of fresh catalysts (**A**) and reduced catalysts (**B**).

2.1.2. TEM

The morphologies of MCM-41, Ni/MCM-41 and Ni-MCM-41 catalysts are tested by Transmission Electron Microscope, as shown in Figure 3. Figure 3A displays uniform porous channel for pure silicon MCM-41 with pore size of 3 nm. For the supported Ni/MCM-41 catalyst, the orderly pore channel still is remained. However, the high temperature calcination in the preparation process has resulted in the formation of large metal particles due to exposure at the outside surface of MCM-41 (Figure 3B). In comparison, the sizes of metal particles within zeolite are smaller for 5%Ni-MCM-41, 10%Ni-MCM-41, and 15%Ni-MCM-41 catalysts due to pore confinement effect of zeolite (Figure 3C–E). Figure 3C displays the Ni particles are located in center part of zeolite rather than the edge position,

indicating that Ni nanoparticles are successfully confined within the channel of MCM-41. As the load amount of Ni increased, the zeolite tends to collapse from margin. It could be obviously observed from 15%Ni-MCM-41 catalyst (Figure 3E). It is deduced that more Ni atoms are connected with Si, resulting in the reducing interaction force among Si-O-Si bond.
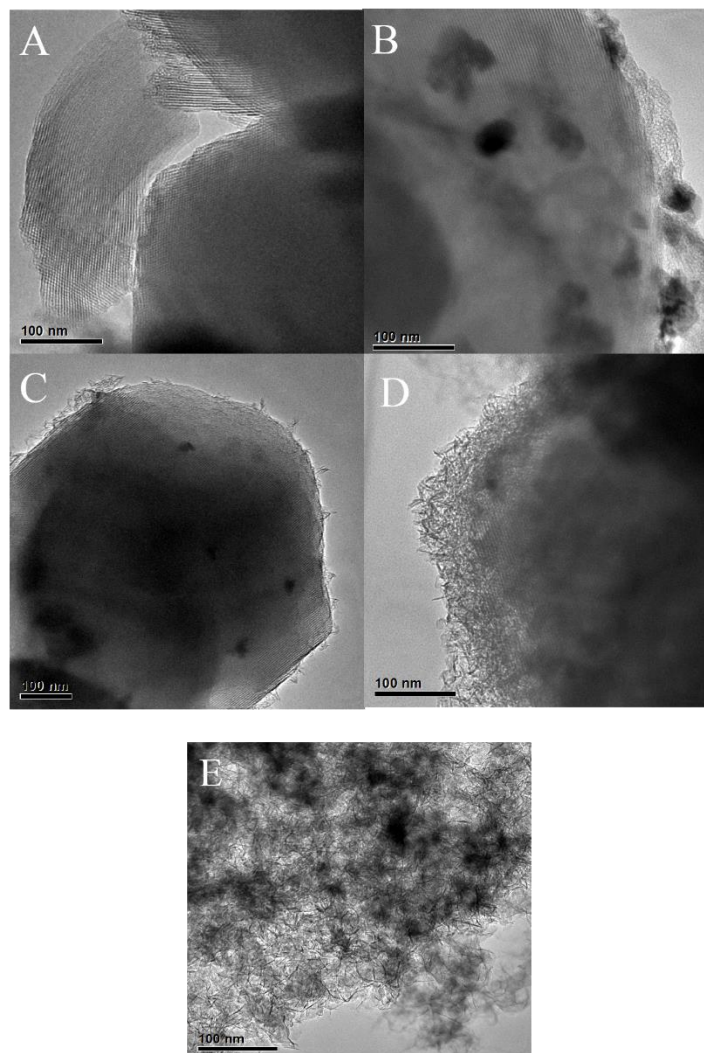

Figure 3. The TEM images of MCM-41 (**A**), reduced 10% Ni/MCM-41 (**B**), reduced 5% Ni-MCM-41 (**C**), reduced 10% Ni-MCM-41 (**D**), and reduced 15% Ni-MCM-41 (**E**).

2.1.3. FT-IR

Figure 4 shows the FT-IR spectrums of fresh MCM-41, Ni/MCM-41, and Ni-MCM-41 catalysts. Vibration peak at 3435 cm^{-1} is assigned to Si-OH and adsorbed water molecules [27]. The peak at 1638 cm^{-1} is attributed to the bending vibration peak of adsorbed water molecules. The vibration peaks at 2925 cm^{-1} and 2854 cm^{-1} are caused by the bending vibration of the electrochemical group $CH(-CH_3)$ and electrochemical group $CH(-CH_2)$. Compared with MCM-41 before calcination, after calcination, the peaks at 2925 cm^{-1} and 2854 cm^{-1} over MCM-41 disappear, indicating that the high temperature treatment can remove template completely. The vibration peaks at 1238 cm^{-1} and 1080 cm^{-1} are the skeleton vibration peaks of MCM-41 mesoporous structure. All the samples show the vibration peaks at this location, indicating that prepared catalysts possessed ordered mesoporous structures. When the amount of Ni increases, the shoulder peak at 960 cm^{-1} weakens gradually for Ni-MCM-41 catalysts.

The reason might be that the introduction of Ni reduces the vibration of Si-O, showing that the Ni within zeolite is connected with the framework.
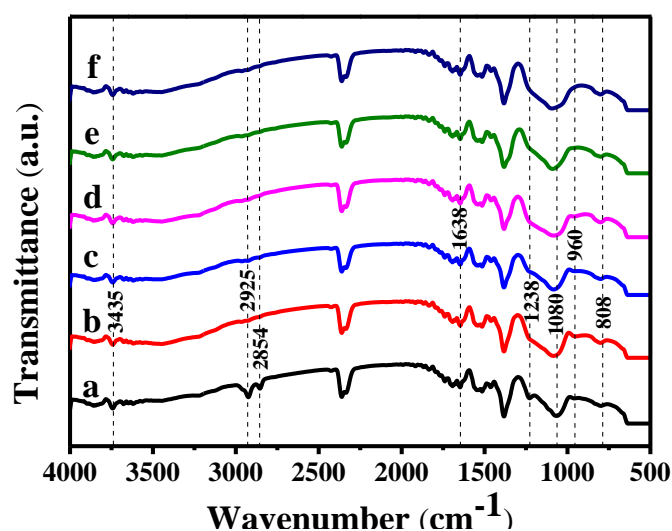

Figure 4. FT-IR spectrums for fresh catalysts. (**a**) MCM-41 before calcination, (**b**) MCM-41 after calcination, (**c**) 10% Ni/MCM-41, (**d**) 5% Ni-MCM-41, (**e**) 10% Ni-MCM-41, and (**f**) 15% Ni-MCM-41.

2.1.4. Location Determination of Ni by ICP

Two existence forms of active metal could be found when they are entering into the zeolite: (1) One is encapsulated into the skeleton of zeolite; and (2) one is located within the pore channel of zeolite. The analysis of XRD, FT-IR, and TEM indicates that the Ni particles are confined within zeolite and some atoms have entered into the skeleton of zeolite. Are there any nickel atoms in the pore channel of zeolite? It needs to be verified. The Ni-MCM-41 catalysts were washed using ammonium acetate solution, which can etch the Ni particles within the pore channel [28,29]. The contents of Ni in catalyst before and after leaching are measured by ICP, and the location of Ni within MCM-41 can be determined. As shown in Table 1, all the amounts of Ni measured before leaching are lower than nominal value, including the Ni within skeleton and channel of zeolite. The amount of Ni measured by ICP after leaching represented that of Ni within skeleton of zeolite. The values within parentheses represented the amounts of Ni within the pore channel of zeolite. The 3.73 wt% of Ni are located within skeleton of zeolite and trace of Ni (0.65 wt%) are dispersed within pore channel. It is deduced that Ni atoms could enter into the skeleton preferentially. When the Ni load amount increased from 5% to 15%, the Ni atoms within the skeleton increased from 3.73 wt% to 8.59 wt%, while the amount of Ni within the channel increased from 0.65 wt% to 4.97 wt%. The result shows more Ni atoms have entered into the skeleton of zeolite. The amounts of Ni within skeleton and pore channel of zeolite increase with the increasing of the load amount.

Table 1. Physicochemical properties of reduced catalysts.

Catalysts	Ni [a] (wt%)	Ni-NH$_4$AC [b] (wt%)	Surface Area [c] (m^2/g)	Pore Volume [d] (cm^3/g)	Pore Size [e] (nm)	TOF$_{CH4}$ [f] (h^{-1})
MCM-41	-	-	978	0.77	2.85	-
5%Ni-MCM-41	4.38	3.73(0.65)	818	0.73	3.31	721.4
10%Ni-MCM-41	8.92	5.74(3.18)	594	0.69	4.77	438.4
15%Ni-MCM-41	13.56	8.59(4.97)	501	0.66	5.37	208.7
10%Ni/MCM-41	9.47	-	566	0.49	2.64	373.5

[a]: Amount of Ni was calculated by ICP before leaching. [b]: Amount of Ni was calculated by ICP after leaching, and the values within parentheses represent the difference before and after leaching. [c]: Calculated by the BET [d]: BJH desorption pore volume [e]: BJH desorption average pore size. [f]: TOF$_{CH4}$ value of POM, mole$_{CH4}$ h^{-1} mole$_{Ni}$$^{-1}$.

The MCM-41 possesses abundant surface area (978 m^2/g). When the introduction amount of Ni increased, the surface area and pore volume decreased due to the blocking of pore channel. Compared with 10%Ni/MCM-41 catalyst, 10%Ni-MCM-41 catalyst has a higher surface area and pore volume, indicating that more Ni atoms were within the skeleton of zeolite rather than the pore channel. It is worth noting that the pore size of Ni-MCM-41 increased with the increasing of Ni amount. Its pore size even was larger than that of MCM-41. The reason might be that the introduction of Ni causes the collapse of segmental pore channel of MCM-41, especially for high load amount (15%Ni-MCM-41).

2.1.5. N$_2$ Adsorption-Desorption

Figure 5 shows N$_2$ adsorption and desorption curves and pore size distributions of Ni/MCM-41 and Ni-MCM-41 catalysts. For 10%Ni/MCM-41 supporting catalyst (Figure 5A), the IV type of isothermal curve is observed, which is highly close to pure MCM-41 material [30,31]. The increase of sharp step at relatively low pressure has suggested capillary condensation inside uniform mesopores [32]. What is more, the steep increase displayed the uniformity of pore sizes. For Ni-MCM-41 catalysts, the N$_2$ uptake rapidly increased at relative pressure range of 0.3–0.5, indicating a typical mesoporous structure. 5%Ni-MCM-41 displayed sharper capillary condensation steps, and it is attributed to more uniform distribution of the pore diameters. The result suggests that the introduction of a low loaded amount of nickel has no damage on the ordered structure of MCM-41. By comparison, milder and milder increases of adsorption-desorption isotherms were observed with increasing loaded amounts of Ni for 10%Ni-MCM-41 and 15%Ni-MCM-41, indicating that the ordered structure of MCM-41 was destroyed gradually.
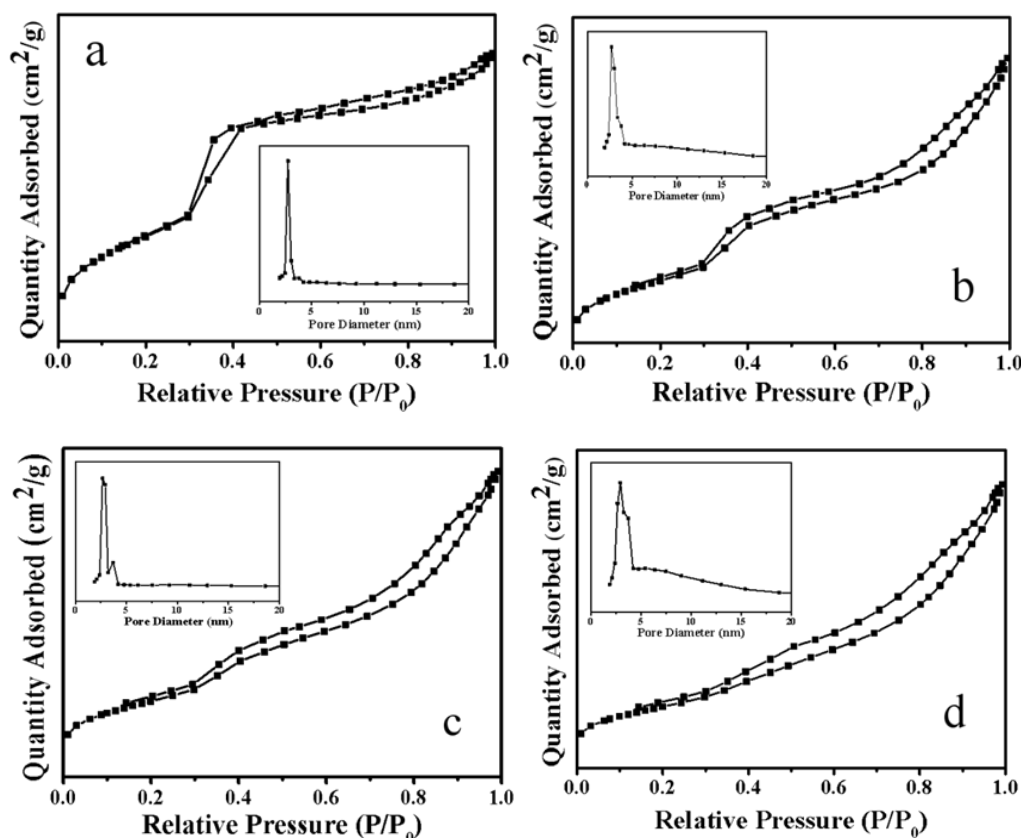

Figure 5. Adsorption-desorption isotherms and pore size distributions of reduced Ni/MCM-41and Ni-MCM-41 catalysts. (**a**) 10%Ni/MCM-41, (**b**) 5%Ni-MCM-41, (**c**) 10%Ni-MCM-41, and (**d**) 15%Ni-MCM-41.

2.1.6. H$_2$-TPR

H$_2$-TPR was conducted to be determined the interaction of Ni species with support. Figure 6 shows that there are two reduction peaks over supported Ni/MCM-41 catalyst. The low temperature peak is around 360 °C with high H$_2$ consumption. The high temperature peak is at 610 °C, indicating most of NiO species possessed weak interaction with MCM-41. MCM-41 could easily cause sintering of Ni metal under the high temperature condition [24]. The speculation is confirmed by the following TEM images. There is only one high temperature reduction peak for 5%Ni-MCM-41. Considering the result of ICP, the reason might be that a large amount of Ni atoms are confined within the skeleton of MCM-41 with strong interaction and hard to be reduced. Two reduction temperature regions are observed when the load amount of Ni increases to 10% or 15%. It is worth noting that the intensity of lower reduction peak increases with the increasing of amount of Ni. Because more NiO atoms enter into pore channel and those are easy to be reduced than those atoms within the skeleton of MCM-41. However, the high temperature reduction peak of 15%Ni-MCM-41 was lower than 10%Ni-MCM-41 catalyst. The result did not agree with ICP result wherein the Ni amount in skeleton (8.59 wt%) over 15%Ni-MCM-41 was higher than that (5.74 wt%) over 10%Ni-MCM-41 catalyst. Based onthe result of TEM, the crystal structure of MCM-41 was destroyed when the load amount of Ni increased to 15 wt%. Though more Ni atoms enter into skeleton of MCM-41, the interaction between Ni and zeolite was weak, resulting in the lower reduction temperature. Compared with Ni/MCM-41 supporting catalyst, the Ni-MCM-41 catalyst has stronger interaction with support, especially 10%Ni-MCM-41 catalyst, which helps to prevent sintering and coking and improves catalytic performance and stability.
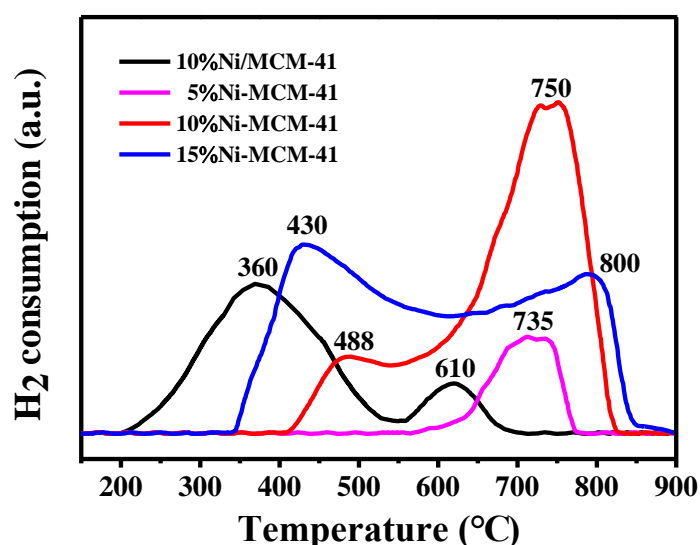

Figure 6. H$_2$-TPR images of fresh Ni/MCM-41 and Ni-MCM-41 catalysts.

2.2. POM Catalytic Activity and Stability

2.2.1. Comparison of Catalytic Performance between Ni/MCM-41 and Ni-MCM-41

Figure 7 displays the comparison of Ni/MCM-41 and Ni-MCM-41 on catalytic performance in POM reaction. Compared with 10%Ni/MCM-41 and other Ni-MCM-41 catalysts, the 10% Ni-MCM-41 showed the highest CH$_4$ conversion. Considering the result of TEM and H$_2$-TPR, 10% Ni-MCM-41 catalyst still maintains the ordered structure of zeolite and a reasonable amount of Ni atoms have entered skeleton of MCM-41, forming strong interaction between Ni and zeolite. Once the reduction occurs, the smaller size of Ni nanoparticles is obtained, which is consistent with XRD result. Catalytic performance of partial oxidation of methane largely depends on the size of active metal [33]. The high dispersibility of Ni provides more outstanding catalytic performance over 10%Ni-MCM-41 catalyst

compared with 10%Ni/MCM-41 catalyst. For 5%Ni-MCM-41 catalyst, ICP result showed 3.73 wt% of Ni entered into skeleton and trace of Ni atoms (0.65 wt%) were located within pore channel of MCM-41. The result indicates that Ni preferentially enters into the zeolite skeleton by isomorphous substitution of silicon. The reduced active sites within zeolite skeleton displayed catalytic activity to some extent. When the loading amount of Ni increased to 15%, the structure of MCM-41 began to collapse and interaction of Ni with zeolite became weak. Once reduced, the larger size of Ni nanoparticles occurred over 15%Ni-MCM-41 catalyst (Figure 2B). These factors explain the CH_4 conversion of Ni-MCM-41 catalysts was in the order of 10%Ni-MCM-41>5%Ni-MCM-41>15%Ni-MCM-41.
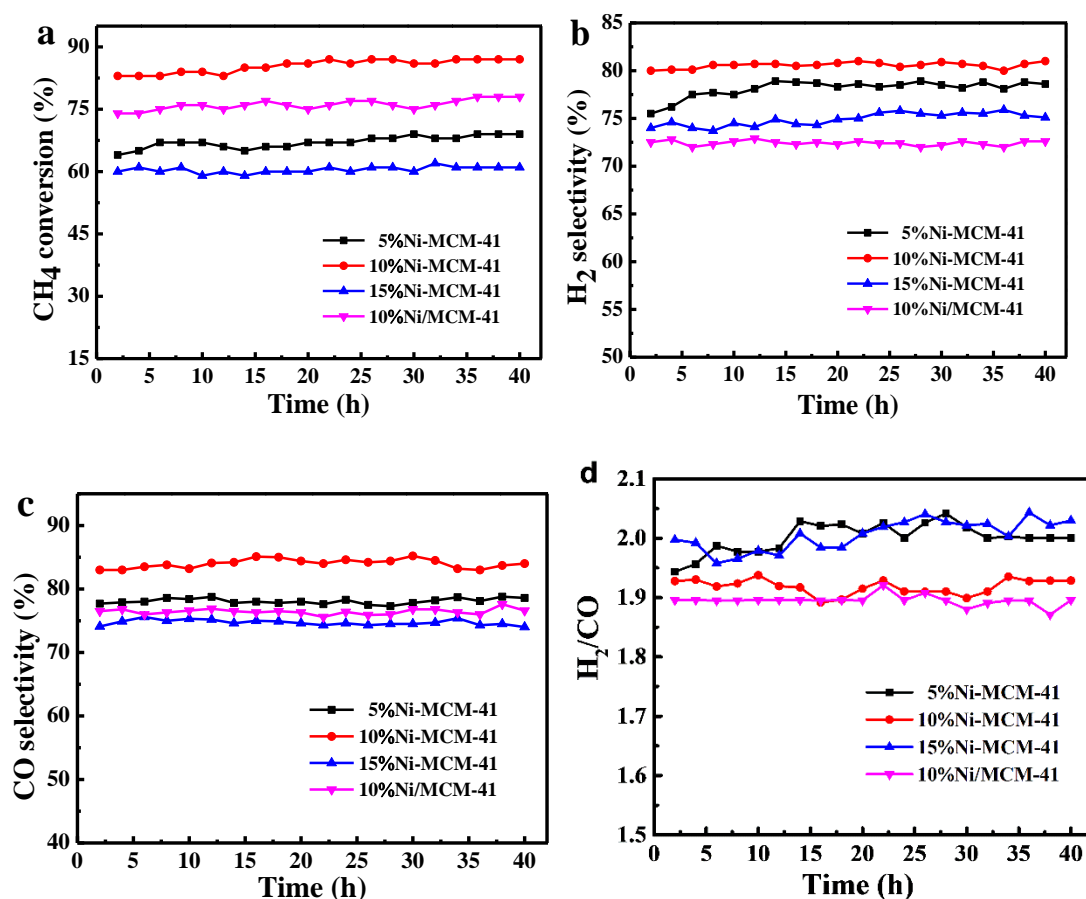

Figure 7. The catalytic ability comparison of the Ni/MCM-41 and Ni-MCM-41 in POM at GHSV = 1.8 × 10^4 mL·g^{-1}·h^{-1}, atmospheric pressure, 750 °C. (**a**) CH_4 conversion, (**b**) H_2 selectivity, (**c**) CO selectivity and (**d**) H_2/CO ratio.

The 10%Ni-MCM-41 catalyst displayed the highest H_2 selectivity among catalysts (Figure 7b). The H_2 selectivity of catalysts followed the order of 10%Ni-MCM-41>5%Ni-MCM-41> 15%Ni-MCM-41>10%Ni/MCM-41. Unfortunately, the supported catalyst showed the lowest H_2 selectivity.

The highest CO selectivity was observed on 10%Ni-MCM-41 catalyst (Figure 7c). The CO selectivities of other catalysts were close (76%). The result was associated to carbon deposition. The confinement effect of MCM-41 on active metal provides limited space for the growth of carbon fiber, 10%Ni/MCM-41 and 5%Ni-MCM-41 catalysts possessed less amount of coking, and high CO selectivity was explained further. Exposed active sites, collapsed zeolite structure and weak interaction of Ni with zeolite framework resulted in severe coking for 10%Ni/MCM-41 and 15%Ni-MCM-41 catalysts, leading to low CO selectivity. The lack of active sites afforded low CO selectivity for 5%Ni-MCM-41 catalyst. Figure 7d showed the H_2/CO ratios of all catalysts were close to

theoretical value (2). Considering the different loaded amount of nickel, the turnover-frequency (TOF) value was calculated based on different CH_4 conversion (Table 1). The TOF was in the order of 5%Ni-MCM-41>10%Ni-MCM-41>10%Ni/MCM-41>15%Ni-MCM-41. 5%Ni-MCM-41 and 10%Ni-MCM-41 catalysts showed superior TOF values, indicating the highly atomic efficiency. For all the Ni-MCM-41 catalysts, it was observed that TOFs increased with decreasing nickel contents. The result displayed suitable nickel content can improve markedly catalytic performances. However, the excessive loaded amount of nickel, for 15%Ni-MCM-41 catalyst, was detrimental to catalytic activity. Compared with 10%Ni/MCM-41 supported catalyst, the nickel confined within the pore channel of MCM-41 afforded outstanding catalytic performance.

The location of active metal inside or outside of mesopore materials significantly affected catalytic activity and selectivity of production. Lanzafame claimed the ZrO_2 was predominantly outside the SBA-15 mesoporous channels for the lower loading, and predominantly inside the mesoporous channels for the higher loading. The acid feature depends on amount of ZrO_2 in SBA-15, which affected catalytic reactivity on HMF etherification with ethanol [34]. Wu compared the Ni catalysts with NiO particles inside or outside the mesopore of MCM-41 for pyrolysis of wood. Due to longer residence time of pyrolysis reactants and high dispersion of the fine NiO particles, the NiO particles located inside mesopore of MCM-41 showed superior catalytic performance, and they could generate more gas and hydrogen and lower oil [35]. For partial oxidation of methane to syngas reaction, the coking over Ni based catalysts was serious due to high diffusion of Ni within nickel metal. The carbon deposition usually started at the binding point between Ni and support and grew to carbon fiber or shell carbon. Selective passivation or coverage of defect, corner atoms, or improving the interaction of metal with support effectively inhibits coking [36]. For Ni-MCM-41 catalysts, nickel was incorporated by isomorphous substitution of silicon in the MCM-41 silica framework, which makes the Ni-MCM-41 a physically stable catalyst in harsh reaction conditions [37]. The suitable Ni atoms like 10%Ni-MCM-41 catalyst preferentially entered the skeleton of MCM-41, forming strong metal-support interactions that contribute to resistance to sintering and coking. This anchoring effect promoted the formation of the active Ni nano-clusters with high dispersion after reduction [38]. The nickel atoms within pore channel also possess outstanding performance due to limited room to prevent coking and sintering.

2.2.2. Catalytic Stability

Due to strong interaction with zeolite framework, the Ni incorporated MCM-41 possessed smaller Ni particles. Contributed by confinement effect of MCM-41, it is speculated that Ni-MCM-41 catalyst owned stable catalytic performance. In order to prove the speculation, more severe condition including higher reaction temperature (800 °C) and GHSV (2.0×10^4 mL·h^{-1}·g^{-1}) were chosen to evaluate catalyst. As shown in Figure 8a, the CH_4 conversion of 10%Ni-MCM-41 catalyst was far higher than 10%Ni/MCM-41 catalyst. The CH_4 conversion of 10%Ni-MCM-41 catalyst was stable with the extended reaction time, while the CH_4 conversion of 10%Ni/MCM-41 catalyst declined. Figure 8b shows that both of CO and H_2 selectivity of 10%Ni-MCM-41 catalyst were higher than those of 10%Ni/MCM-41 catalyst. It is worth noting that CO and H_2 selectivity of 10%Ni/MCM-41 catalyst were decreasing. It is speculated that the growth-up of nickel nanoparticle and carbon deposition resulted in decline of catalytic activity. The results indicated the Ni incorporated MCM-41 catalyst had excellent anti-carbon and coking ability, and stability of catalyst was improved due to the confinement effect of zeolite. 5%Ni-MCM-41 catalyst was also tested for catalytic stability in view of low carbon deposition. As shown in Figure 8, 5%Ni-MCM-41 catalyst showed outstanding catalytic stability for 100 h, however, its catalytic activity was lower than 10%Ni-MCM-41 catalyst due to low loading amount of Ni. Figure 8d shows the H_2/CO ratios of all catalysts were close to 2 (theoretical value).
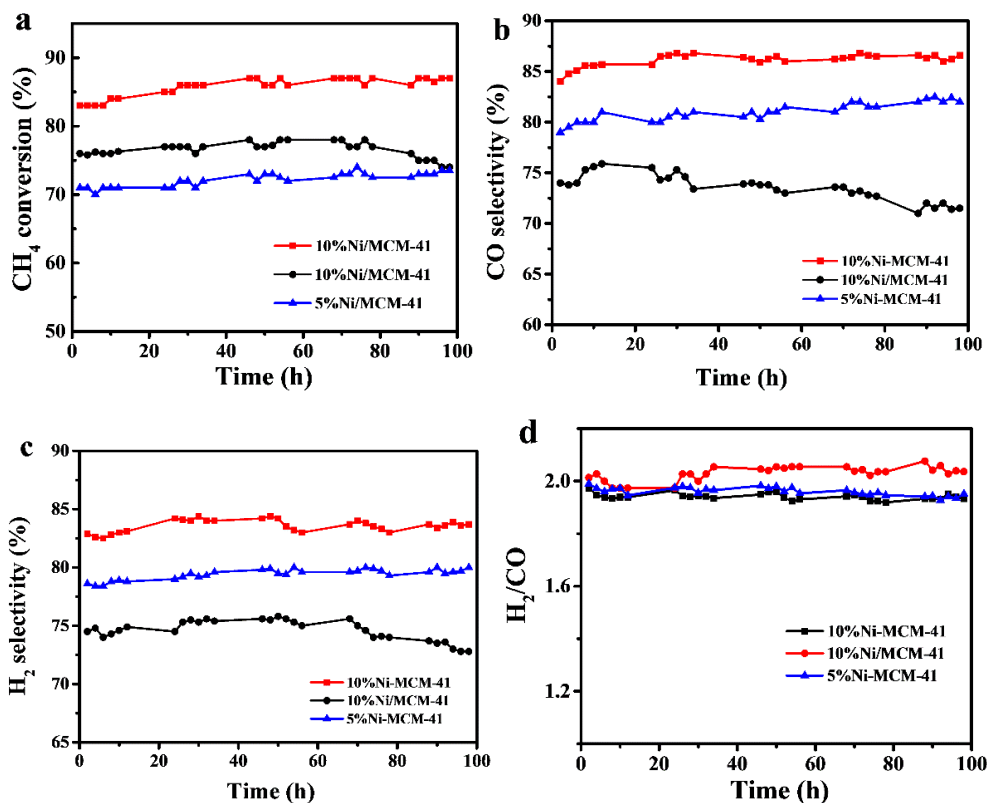
Figure 8. Stability test of 10%Ni-MCM-41 and 10%Ni/MCM-41 catalysts in POM at GHSV = 2.0 × 10^4 mL·h^{-1}·g^{-1}, atmospheric pressure, 800 °C. (**a**) CH$_4$ conversion, (**b**) CO selectivity, (**c**) H$_2$ selectivity and (**d**) H$_2$/CO ratio.

2.3. Characterization after Tests

2.3.1. Phase Composition

As shown in Figure 9, both of the NiO and Ni species can be observed from the spent catalyst, which is consistent with previous reports [39]. Compared with the sharp diffraction of NiO in 10%Ni/MCM-41 spent catalyst, the intensity of NiO in 10%Ni-MCM-41 spent catalyst was lower. The result suggested the Ni metal was confined within the channel of zeolite and the confinement successfully prevented the sintering of active metal under harsh conditions.
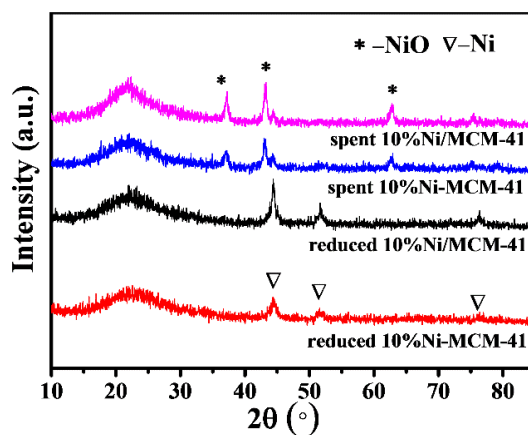

Figure 9. Wide angle XRD patterns comparation of reduced and spent 10%Ni/MCM-41 and 10%Ni-MCM-41 catalysts.

2.3.2. TEM

Figure 10A shows obvious growth-up of Ni nanoparticles (about 85 nm) and occurred for spent 10%Ni/MCM-41 catalyst compared to reduced 10%Ni/MCM-41 catalyst in Figure 3B. The severe sintering of Ni was observed due to weak interaction with support and exposure under harsh conditions. On the contrary, due to confinement of MCM-41, size of Ni nanoparticles in spent 10%Ni-MCM-41 catalyst slightly increased, and excellent sintering resistance was observed (Figure 10B).
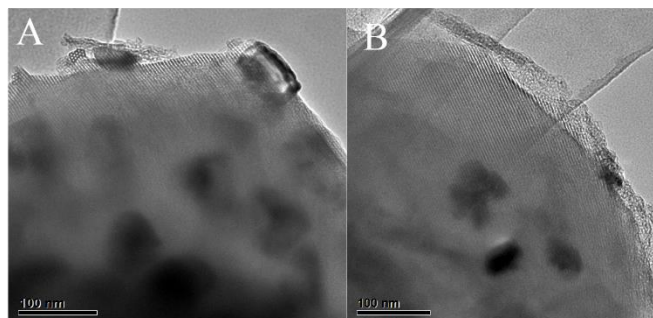

Figure 10. The TEM images of spent 10%Ni/MCM-41 (**A**) and spent 10%Ni-MCM-41 (**B**).

2.3.3. TGA

Carbon deposition is prone to occur on nickel-based catalyst at high temperature, which is one of the important reasons for catalyst deactivation. The methane cracking and the Boudouard reaction stand out in the hypothesis about the mechanism of coke formation. The report suggested the carbon deposition from methane cracking occur at high temperature (>814 K). However, coke formation most likely take place from Boudouard reaction at temperature (<977 K) [40]. Therefore, the coking is difficult to avoid thermodynamically.

$$CH_4 \rightarrow C + 2H_2 \qquad \Delta H = 74.8 \text{ kJ mol}^{-1} \qquad \text{(methane cracking)}$$
$$2CO \rightarrow C + CO_2 \qquad \Delta H = -172.8 \text{ kJ mol}^{-1} \qquad \text{(Boudouard reaction)}$$
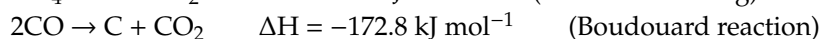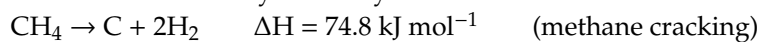
Figure 11 shows the weight loss of spent Ni/MCM-41 and Ni-MCM-41 catalysts. The weights of all spent catalysts began to reduce at 450 °C, which was attributed to oxidation of surface carbon species [41]. Compared with Ni/MCM-41 catalyst, the Ni-MCM-41 catalysts possessed lower coking, especially 5%Ni-MCM-41 catalyst. The amount of coking increased with increasing of Ni load amount. Combining with previous analysis, it is deduced that the Ni species within the skeleton contributed to coking inhibition than those within the pore channel.
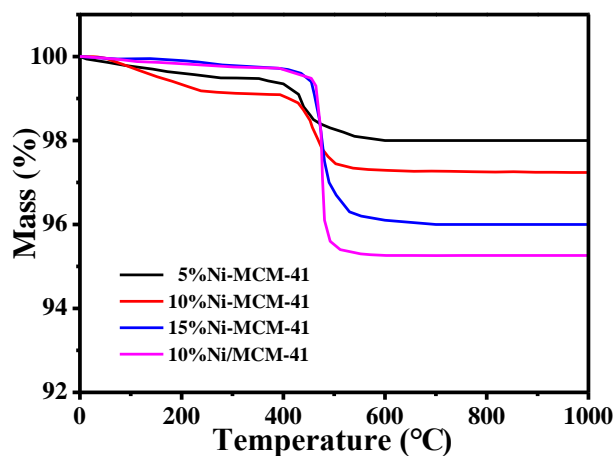

Figure 11. TGA of spent Ni/MCM-41 and Ni-MCM-41 catalysts.

Due to the similar TG curve, the DTG curves of all the spent catalysts were compared. As shown in Figure 12, the weight loss temperatures of all catalysts were in the order of 5%Ni-MCM-41<10%Ni-MCM-41<15%Ni-MCM-41<10%Ni/MCM-41. The fasted weight loss temperature slightly increased with increasing the loaded amount of Ni for Ni-MCM-41 catalysts. It is well known that insert carbon requires much oxidization temperature. The result indicated the insert carbon easily occurred at high-loading sample and supported catalyst [42]. Based on the characterization results reported elsewhere [43,44], the graphic-like carbon should be deposited onto 15%Ni-MCM-41 and 10%Ni/MCM-41, however, no diffraction peak was observed in XRD due to trace amount of coking. On contrast, the low temperature peaks (around 200 °C) were observed in DTG curves of 5%Ni-MCM-41 and 10%Ni-MCM-41 catalysts, indicating the existence of active carbon or amorphous carbon.
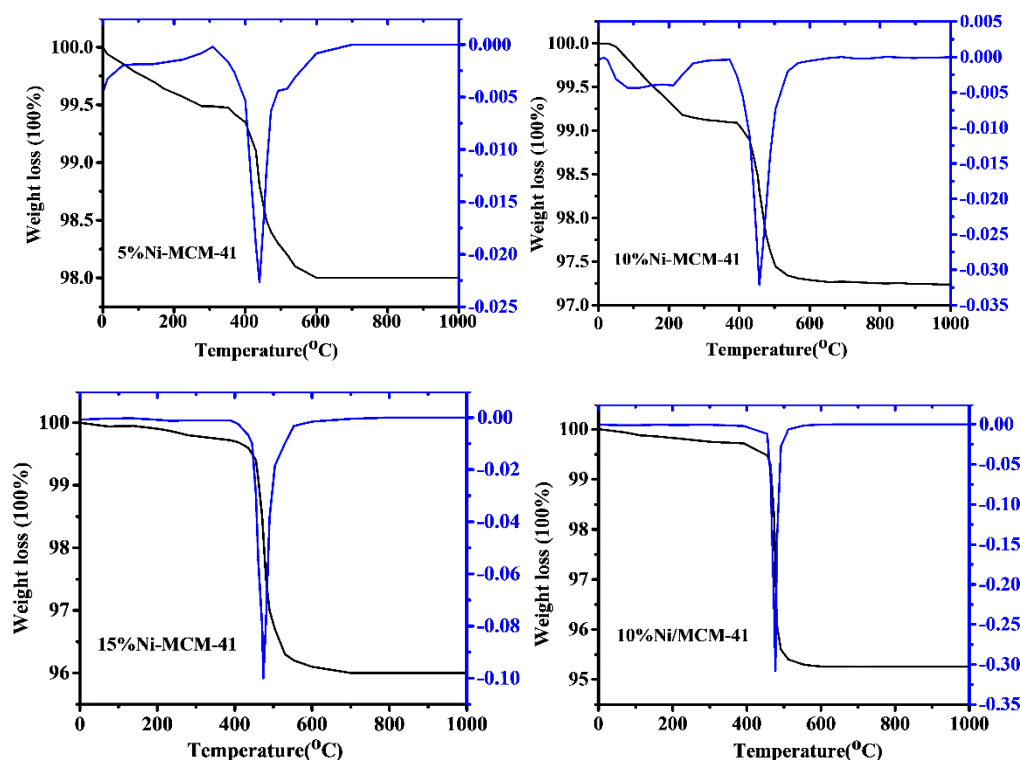

Figure 12. DTG of spent Ni/MCM-41 and Ni-MCM-41 catalysts.

3. Experimental

3.1. Materials

Cetyl trimethyl ammonium bromide (CTAB, AR), nickel nitrate, ammonium hydroxide (AR), tetraethoxysilane (TEOS, AR) were purchased from Aladdin biochemical technology co., LTD (Shanghai, China). All the reagents were used without secondary purification. Deionized water was produced via Milli-Q Academic.

3.2. Preparation of Catalysts

The Ni-MCM-41 catalysts were prepared via hydrothermal synthesis method. Taking 10%Ni-MCM-41 catalyst as an example, the 2.345 g of cetyl trimethyl ammonium bromide (CTAB) was dissolved in 100 mL of deionized water. The mixture was named solution A after stirring for 0.5 h with 800 r/min at 25 °C. 0.77 g of nickel nitrate was dissolved in 20 mL of deionized water and added dropwise ammonium hydroxide to adjust the pH of solution to 10 to form solution B. Solution B was slowly poured into solution A with stirring at 800 r/min. After 30 min, 10 mL of tetraethoxysilane

(TEOS) was added dropwise into the mixture to adjust the pH of solution to 10. The obtained solution was transfer into to an autoclave of 200 mL and heated at 110 °C with rate of 5 °C/min for 48 h. After hydrothermal crystallization, to remove presumable excess ions, the sample was washed by 50 mL of deionized water twice and dried at 70 °C overnight, calcined at 550 °C with rate of 10 °C/min for 6 h under air atmosphere. Others catalysts were prepared via similar method except different amount of nickel nitrate. The molar ratio of SiO_2:CTAB:NH_3:Ni:H_2O was 1:0.152:2.8:x:141.2 (x = 0.05, 0.1, 0.15 for different loading amounts of Ni). The obtained samples were named as xNi-MCM-41 (x = 5%, 10%, 15%), respectively.

The MCM-41 zeolite was prepared by similar method without adding nickel nitrate. The Ni supported MCM-41 catalysts were prepared by impregnation method. 0.622 g of nickel nitrate was dissolved in 2 mL of deionized water. 2 g of MCM-41 zeolite was added into prepared solution at aid of ultrasonic. The obtained sample was dried at 70 °C over night, calcined at 550 °C with the rate of 10 °C/min for 6 h under air atmosphere. The obtained sample was named as 10%Ni/MCM-41 catalyst.

3.3. Catalyst Characterization

The specific surface area and pore size distribution measure were conducted by QUADRSORB SI with P/P_0 range from 0.0096 to 0.9944. The degassed treatment for 3 h at 300 °C was required firstly. The result of surface area was obtained via multipoint BET analysis of the N_2 adsorption isotherms. Pore size distribution was obtained based on desorption isotherm branch. SHIMADZU-6000 powder diffractometer (Shimadzu, Tokyo, Japan) with Cu Kα radiation was employed to obtain X-ray powder diffraction (XRD) results with scan rate of 10°/min. The TEM images were taken over a JEOL JEM-2010 instrument (JEOL, Tokyo, Japan) operated at 100 kV. To obtain the spent catalysts, the reactant flows were stopped simultaneously and switched to He flow of 60 mL/min. The catalysts were then flushed and cooled in He before being sealed. The amount of coking was characterized via TA Q600 TG analyzer (TA, Delaware, USA). Inductive coupled plasma (ICP) technique (Agilent 7700, Agilent, California, USA) was employed to measure nickel contents of the samples. The HF solution was used to dissolve the sample before test. The Thermo Nicolet Nexus FT-IR470 spectrometer (Thermo Fisher Scientific, Massachusetts, USA) afforded Fourier transform infrared (FT-IR) spectra of samples with MCT detector. Wafer (diameter: 13 mm; weight: 200 mg) was obtained by tableting and scanned range from 500 cm^{-1} to 4000 cm^{-1}. The interaction between metal and support was determined by the H_2 TPR technique. 30 mg of catalysts were fixed in quartz reactor and reduced under 25% H_2/N_2 (V/V, 60 mL/min) flow with increasing temperature from room temperature to 900 °C at a rate of 10 °C/min. Outlet gas was monitored by a thermal conductive detector.

3.4. Catalyst Evaluation

The catalytic performance was measured within tubular quartz reactor (inner diameter of 10 mm, length of 110 cm). The catalyst was sieved to 20–40 mesh before test. The 0.5 g of catalyst were fixed in the middle of reactor by two quartz wool beds. The electric power was employed to supply heat energy and temperature of catalyst bed was controlled via thermocouple in the middle of reactor. Then CH_4 and O_2 mixture (V/V = 2/1, 99.99%, 99.99% of purity) flowed through reactor with 5×10^4 mL·h^{-1}·g^{-1} at atmospheric pressure. The effluent gas composition was determined by gas chromatograph (Haixin GC 920, Haixin, Shanghai, China) equipped with TCD and FID detector. H_2, O_2 and CH_4 were detected by TCD detector through column of 5A zeolite molecular sieve. CO, CH_4 and CO_2 were detected by FID detector through column of carbon molecular sieve with reforming reactor. The data from two detectors were correlated by CH_4. The catalysts were reduced before activity test. The catalysts were reduced under 25% H_2/N_2 (V/V, 80 mL/min) flow with temperature increasing from 25 °C to 800 °C (determined from H_2-TPR) for 2 h. The equations of conversion or selectivity were shown as follows:

Conversion of CH_4 = $(F_{in\text{-}CH4} - F_{out\text{-}CH4})/F_{in\text{-}CH4} \times 100\%$

Selectivity of CO = $F_{out\text{-}CO}/(F_{in\text{-}CH4} - F_{out\text{-}CH4}) \times 100\%$

Selectivity of H_2 = $F_{out\text{-}H2}/2(F_{in\text{-}CH4} - F_{out\text{-}CH4}) \times 100\%$

Ratio of $H_2/CO = F_{out-H2}/F_{out-CO}$
F-volume flow rate, mL/min

4. Conclusions

The well-ordered Ni-MCM-41 catalysts with different nickel content were synthesized by a direct hydrothermal method. The results indicated that the nickel atoms preferentially entered into the framework with tetrahedral coordination. The incorporated Ni atoms increased with the increasing of the load amount of Ni. The Ni particles of Ni-MCM-41 catalysts were highly dispersed with smaller particle size compared with supported Ni/MCM-41 catalyst, especially 10%Ni-MCM-41 catalyst. Compared with supported 10%Ni/MCM-41 catalyst, the higher CH_4 conversion, production selectivity and longer catalyst life were obtained. The improved catalytic performance was suggested to closely associate with both the amounts of active centers on the pore wall surface and the stabilized dispersion of these active sites by the silica matrix.

Author Contributions: Software, Q.M.; formal analysis, J.G.; investigation, Z.M.; data curation, Y.L.; L.M.; writing—original draft preparation, C.D.; supervision, J.W.; P.L.

Conflicts of Interest: The authors declare no conflict of interest.

References

1. Sattler, J.J.H.B.; Gonzalez-Jimenez, I.D.; Luo, L.; Stears, B.A.; Malek, A.; Barton, D.G.; Kilos, B.A.; Kaminsky, M.P.; Verhoeven, T.W.G.M.; Koers, E.J.; et al. Platinum-Promoted Ga/Al2O3as Highly Active, Selective, and Stable Catalyst for the Dehydrogenation of Propane. *Angew. Chem.* **2014**, *126*, 9405–9410. [CrossRef]

2. Guo, C.; Zhang, X.; Zhang, J.; Wang, Y. Preparation of La2NiO4 catalyst and catalytic performance for partial oxidation of methane. *J. Mol. Catal. A: Chem.* **2007**, *269*, 254–259. [CrossRef]

3. Bonura, G.; Migliori, M.; Frusteri, L.; Cannilla, C.; Catizzone, E.; Giordano, G.; Frusteri, F. Acidity control of zeolite functionality on activity and stability of hybridcatalysts during DME production via CO_2 hydrogenation. *J. CO2 Util.* **2018**, *24*, 398–406. [CrossRef]

4. Perathoner, S.; Centi, G. CO2Recycling: A Key Strategy to Introduce Green Energy in the Chemical Production Chain. *ChemSusChem* **2014**, *7*, 1274–1282. [CrossRef] [PubMed]

5. Catizzone, E.; Cirelli, Z.; Aloise, A.; Lanzafame, P.; Migliori, M.; Giordano, G. Methanol conversion over ZSM-12, ZSM-22 and EU-1 zeolites: from DME to hydrocarbons production. *Catal. Today* **2018**, *304*, 39–50. [CrossRef]

6. Horiguchi, J.; Kobayashi, Y.; Kobayashi, S.; Yamazaki, Y.; Omata, K.; Nagao, D.; Konno, M.; Yamada, M. Mesoporous NiO–Al2O3 catalyst for high pressure partial oxidation of methane to syngas. *Appl. Catal. A: Gen.* **2011**, *392*, 86–92. [CrossRef]

7. Singha, R.K.; Shukla, A.; Yadav, A.; Konathala, L.N.S.; Bal, R. Effect of metal-support interaction on activity and stability of Ni-CeO2 catalyst for partial oxidation of methane. *Appl. Catal. B-Environ.* **2017**, *202*, 473–488. [CrossRef]

8. Argyle, M.D.; Bartholomew, C.H. Heterogeneous catalyst deactivation and regeneration: A review. *Catalysts* **2015**, *5*, 145–269. [CrossRef]

9. Ding, C.; Ai, G.; Zhang, K.; Yuan, Q.; Han, Y.; Ma, X.; Wang, J.; Liu, S. Coking resistant Ni/ZrO$_2$@SiO$_2$ catalyst for the partial oxidation of methane to synthesis gas. *Int. J. Hydrog. Energy* **2015**, *40*, 6835–6843. [CrossRef]

10. Özdemir, H.; Öksüzömer, M.A.F.; Gürkaynak, M.A. Effect of the calcination temperature on Ni/MgAl$_2$O$_4$ catalyst structure and catalytic properties for partial oxidation of methane. *Fuel* **2014**, *116*, 63–70. [CrossRef]

11. Vartuli, J.C.; Roth, W.J.; Degnan, T.F. Mesoporous Materials (M41S): From Discovery to Application. In *Dekker Encyclopedia of Nanoscience and Nanotechnology*; Marcel Dekker: New York, NY, USA, 2004; p. 1791.

12. Gucbilmez, Y.; Doğu, T.; Balci, S. Ethylene and Acetaldehyde Production by Selective Oxidation of Ethanol Using Mesoporous V−MCM-41 Catalysts. *Ind. Eng. Chem. Res.* **2006**, *45*, 3496–3502. [CrossRef]

13. Sener, C.; Doğu, T.; Dogu, G. Effects of synthesis conditions on the structure of Pd incorporated MCM-41 type mesoporous nanocomposite catalytic materials with high Pd/Si ratios. *Microporous Mesoporous Mater.* **2006**, *94*, 89–98. [CrossRef]

14. Yasyerli, S.; Filizgok, S.; Arbag, H.; Yasyerli, N.; Dogu, G. Ru incorporated Ni–MCM-41 mesoporous catalysts for dry reforming of methane: Effects of Mg addition, feed composition and temperature. *Int. J. Hydrog. Energy* **2011**, *36*, 4863–4874. [CrossRef]

15. Arbag, H.; Yaşyerli, S.; Yasyerli, N.; Dogu, G. Activity and stability enhancement of Ni-MCM-41 catalysts by Rh incorporation for hydrogen from dry reforming of methane. *Int. J. Hydrog. Energy* **2010**, *35*, 2296–2304. [CrossRef]

16. Qin, J.; Li, B.; Zhang, W.; Lv, W.; Han, C.; Liu, J. Synthesis, characterization and catalytic performance of well-ordered mesoporous Ni-MCM-41 with high nickel content. *Microporous Mesoporous Mater.* **2015**, *208*, 181–187. [CrossRef]

17. Liu, H.M.; Li, Y.M.; Wu, H.; Yang, W.W.; He, D.H. Promoting effect of glucose and b-cyclodextrin on Ni dispersion of Ni/MCM-41 catalysts for carbon dioxide reforming of methane to syngas. *Fuel* **2014**, *136*, 19–24. [CrossRef]

18. Qiu, S.; Xu, Y.; Weng, Y.; Ma, L.; Wang, T. Efficient Hydrogenolysis of Guaiacol over Highly Dispersed Ni/MCM-41 Catalyst Combined with HZSM-5. *Catalysts* **2016**, *6*, 134. [CrossRef]

19. Yang, Y.; Lim, S.; Du, G.; Chen, Y.; Ciuparu, D.; Haller, G.L. Synthesis and Characterization of Highly Ordered Ni-MCM-41 Mesoporous Molecular Sieves. *J. Phys. Chem. B* **2005**, *109*, 13237–13246. [CrossRef]

20. Al-Fatesh, A.S.; Ibrahim, A.A.; Abu-Dahrieh, J.K.; Al-Awadi, A.S.; El-Toni, A.M.; Fakeeha, A.H.; Abasaeed, A.E. Gallium-Promoted Ni Catalyst Supported on MCM-41 for Dry Reforming of Methane. *Catalysts* **2018**, *8*, 229. [CrossRef]

21. Du, G.; Lim, S.; Yang, Y.; Wang, C.; Pfefferle, L.; Haller, G.L. Methanation of carbon dioxide on Ni-incorporated MCM-41 catalysts: The influence of catalyst pretreatment and study of steady-state reaction. *J. Catal.* **2007**, *249*, 370–379. [CrossRef]

22. Li, X.-K.; Ji, W.-J.; Zhao, J.; Wang, S.-J.; Au, C.T. Ammonia decomposition over Ru and Ni catalysts supported on fumed SiO$_2$, MCM-41, and SBA-15. *J. Catal.* **2005**, *236*, 181–189. [CrossRef]

23. Parvulescu, V.; Su, B.-L. Iron, cobalt or nickel substituted MCM-41 molecular sieves for oxidation of hydrocarbons. *Catal. Today* **2001**, *69*, 315–322. [CrossRef]

24. Yang, Y.; Lim, S.; Du, G.; Wang, C.; Ciuparu, D.; Chen, Y.; Haller, G.L. Controlling of Physicochemical Properties of Nickel-Substituted MCM-41 by Adjustment of the Synthesis Solution pH and Tetramethylammonium Silicate Concentration. *J. Phys. Chem. B* **2006**, *110*, 5927–5935. [CrossRef] [PubMed]

25. Long, J.; Liu, G.H.; Cheng, T.Y.; Yao, H.; Qian, Q.Q.; Zhuang, J.L.; Gao, F.; Li, H.X. Immobilization of rhodium-based transfer hydrogenation catalysts on mesoporous silica materials. *J. Catal.* **2013**, *298*, 41–50. [CrossRef]

26. Nares, R.; Ramírez, J.; Gutiérrezalejandre, A.; Cuevas, R. Characterization and hydrogenation activity of Ni/Si(Al)-MCM-41 catalysts prepared by deposition−precipitation. *J. Eletrochem. Soc.* **2010**, *128*, 1062–1064. [CrossRef]

27. Jiang, T.; Tang, Y.; Zhao, Q.; Yin, H. Effect of Ni-doping on the pore structure of pure silica MCM-41 mesoporous molecular sieve under microwave irradiation. *Colloids Surfaces A Physicochem. Eng. Asp.* **2008**, *315*, 299–303. [CrossRef]

28. Sakthivel, A.; Dapurkar, S.E.; Selvam, P. Mesoporous (Cr)MCM-41 and (Cr)MCM-48 Molecular Sieves: Promising Heterogeneous Catalysts for Liquid Phase Oxidation Reactions. *Catal. Lett.* **2001**, *77*, 155–158. [CrossRef]

29. Barrett, P.A.; Sankar, G.; Catlow, C.R.A.; Thomas, J.M. X-ray absorption spectroscopic study of Bønsted, Lewis, and redox centers in cobalt-substituted aluminum phosphate catalysts. *J. Phys. Chem.* **1996**, *100*, 8977–8985. [CrossRef]

30. Corma, A.; Fornes, V.; Navarro, M.; Perezpariente, J. Acidity and Stability of MCM-41 Crystalline Aluminosilicates. *J. Catal.* **1994**, *148*, 569–574. [CrossRef]

31. Biz, S.; Occelli, M.L. Synthesis and Characterization of Mesostructured Materials. *Catal. Rev.* **1998**, *40*, 329–407. [CrossRef]

32. Catizzone, E.; Van Daele, S.; Bianco, M.; Di Michele, A.; Aloise, A.; Migliori, M.; Valtchev, V.; Giordano, G. Catalytic application of ferrierite nanocrystals in vapour-phase dehydration of methanol to dimethyl ether. *Appl. Catal. B Environ.* **2019**, *243*, 273–282. [CrossRef]

33. Kondratenko, V.A.; Berger-Karin, C.; Kondratenko, E.V. Partial oxidation of methane to syngas over γ-Al2O3-supported Rh nanoparticles: Kinetic and mechanistic origins of size effect on selectivity and activity. *ACS Catal.* **2014**, *4*, 3136–3144. [CrossRef]

34. Barbera, K.; Lanzafame, P.; Pistone, A.; Millesi, S.; Malandrino, G.; Gulino, A.; Perathoner, S.; Centi, G. The role of oxide location in HMF etherification with ethanol over sulfated ZrO_2 supported on SBA-15. *J. Catal.* **2015**, *323*, 19–32. [CrossRef]

35. Wu, C.; Dong, L.; Onwudili, J.; Williams, P.T.; Huang, J. Effect of Ni Particle Location within the Mesoporous MCM-41 Support for Hydrogen Production from the Catalytic Gasification of Biomass. *ACS Sustain. Chem. Eng.* **2013**, *1*, 1083–1091. [CrossRef]

36. Lu, J.; Fu, B.; Kung, M.C.; Xiao, G.; Elam, J.W.; Kung, H.H.; Stair, P.C. Coking- and Sintering-Resistant Palladium Catalysts Achieved Through Atomic Layer Deposition. *Science* **2012**, *335*, 1205–1208. [CrossRef] [PubMed]

37. Komatsu, T.; Kishi, T.; Gorai, T. Preparation and catalytic properties of uniform particles of Ni_3Ge intermetallic compound formed inside the mesopores of MCM-41. *J. Catal.* **2008**, *259*, 174–182. [CrossRef]

38. Liu, D.; Lau, R.; Borgna, A.; Yang, Y. Carbon dioxide reforming of methane to synthesis gas over Ni-MCM-41 catalysts. *Appl. Catal. A: Gen.* **2009**, *358*, 110–118. [CrossRef]

39. Rabe, S.; Nachtegaal, M.; Vogel, F. Catalytic partial oxidation of methane to synthesis gas over a ruthenium catalyst: The role of the oxidation state. *Phys. Chem. Chem. Phys.* **2007**, *9*, 1461. [CrossRef]

40. Ding, C.; Wang, J.; Jia, Y.; Ai, G.; Liu, S.; Liu, P.; Zhang, K.; Han, Y.; Ma, X. Anti-coking of Yb-promoted Ni/Al2O3 catalyst in partial oxidation of methane. *Int. J. Hydrog. Energy* **2016**, *41*, 10707–10718. [CrossRef]

41. Nair, M.M.; Kleitz, F.; Kaliaguine, S. Kinetics of Methanol Oxidation over Mesoporous Perovskite Catalysts. *ChemCatChem* **2012**, *4*, 387–394. [CrossRef]

42. Cakiryilmaz, N.; Arbag, H.; Oktar, N.; Dogu, G.; Dogu, T. Catalytic performances of Ni and Cu impregnated MCM-41 and Zr-MCM-41 for hydrogen production through steam reforming of acetic acid. *Catal. Today* **2019**, *323*, 191–199. [CrossRef]

43. Wang, S.B.; Lu, G.Q. A Comprehensive Study on Carbon Dioxide Reforming of Methane over Ni/γ-Al$_2$O$_3$ Catalysts. *Ind. Eng. Chem. Res.* **1999**, *38*, 2615–2625. [CrossRef]

44. Bradford, M.C.; Vannice, M.A. Catalytic reforming of methane with carbon dioxide over nickel catalysts I. Catalyst characterization and activity. *Appl. Catal. A Gen.* **1996**, *142*, 73–96. [CrossRef]